

Calculation of Raman spectra and vibrational properties of silicate glasses: Comparison between $\text{Na}_2\text{Si}_4\text{O}_9$ and SiO_2 glasses

N. Zotov

Bayerisches Geoinstitut, D-95440 Bayreuth, Germany

I. Ebbsjö

Studsvik Neutron Research Laboratory, S-61182 Nyköping, Sweden

D. Timpel

Max-Planck Institut für Microsystems, D-06120 Halle, Germany

H. Keppeler

Bayerisches Geoinstitut, D-95440 Bayreuth, Germany

(Received 16 November 1998; revised manuscript received 4 May 1999)

First calculations of the vibrational density of states (VDOS), the character of the vibrational modes, and the polarized Raman spectra of depolymerized alkali silicate glass with 20 mol % Na_2O ($\text{Na}_2\text{Si}_4\text{O}_9$ glass) using Kirkwood-type potential and computer generated models with periodic boundary conditions are presented and compared with amorphous SiO_2 ($a\text{-SiO}_2$). The effects of depolymerization on the localization, bridging oxygen motion, phase quotient, as well as the newly proposed stretching character and atomic participation ratios of the vibrational modes are quantitatively analyzed. The band edges are shown to correspond to strongly localized modes. All vibrational characteristics have singularities near the band edges. The calculated Raman spectra are, generally, in good agreement with experiment. The parallel (VV) polarized Raman spectra are shown to arise mainly from a bond-stretching scattering mechanism which depends on the derivative of the parallel bond polarizability. On the contrary, the depolarized VH spectra arise from mixed bond-stretching and bond-bending scattering mechanisms. It is shown that the perpendicular polarizability of the silicon-bridging oxygen bonds is an order of magnitude smaller than the derivative of the parallel bond polarizability and that their ratio of about 0.1 is not affected by the presence of short-range disorder and depolymerization. The derivative of the parallel bond polarizability for the silicon-nonbridging oxygen bonds is twice larger than that for the silicon-bridging oxygen bonds. Partial Raman spectra of short-range units with different number of nonbridging oxygens (Q species) in the $\text{Na}_2\text{Si}_4\text{O}_9$ glass are calculated and compared with empirically established rules for determination of Q species from polarized Raman spectra. [S0163-1829(99)01333-8]

I. INTRODUCTION

Considerable progress has been made in the theoretical understanding of the vibrational properties of silicate glasses. Most of the work done so far is on the vibrational density of states (VDOS) of amorphous SiO_2 ($a\text{-SiO}_2$). VDOS calculations on $a\text{-SiO}_2$ have been performed using various types of computational methods: the inverse iteration method,¹ direct diagonalization of the dynamical matrix,²⁻⁸ Fourier transform of the velocity-velocity autocorrelation function,⁹⁻¹³ the Bethe lattice model,^{14,15} and the central-force model of Sen and Thorpe.^{16,17}

However, despite the fact that Raman and infrared (IR) spectra are very sensitive probes of the local structure of amorphous materials, there are only a few calculations of the Raman and IR spectra of $a\text{-SiO}_2$, mainly due to the fact that the coupling coefficients linking these optical spectra with the VDOS are strong functions of the vibrational frequency.¹⁸⁻²⁰ Bell and Hibbins-Butler have calculated the IR spectra²¹ using a point-charge model and the Raman spectra²² using the bond polarizability approximation of $a\text{-SiO}_2$ for selected equidistantly distributed frequencies

from their hand-built random network model with free and fixed boundary conditions. The IR and Raman spectra of small $a\text{-SiO}_2$ clusters with Bethe lattice boundary conditions were calculated analytically using the Green's-function approach.^{14,15} More recently, the IR spectra of $a\text{-SiO}_2$ models with periodic boundary conditions were calculated numerically using the point-charge model with effective charges obtained from electronic calculations,³ using the current-current autocorrelation function²³ taking into account the contribution of the induced dipoles and from the transverse dielectric response function using Born charges derived from first principles.²⁴ Good agreement with experiment was found both for the positions and the intensities of the main IR peaks.^{23,24} The only realistic calculation of the Raman spectra of $a\text{-SiO}_2$ model with periodic boundary conditions, to the best of our knowledge, is the work of Murray and Ching³ using the bond polarizability approximation and direct diagonalization of the whole dynamical matrix.

Beyond $a\text{-SiO}_2$, the interpretation of the Raman and IR spectra of binary and multicomponent silicate glasses is still essentially on a qualitative level despite the enormous amount of experimental vibrational spectra published and

their importance both in material and earth sciences. Various empirical rules are currently used for structural interpretation of the glass spectra. They are based on comparison of Raman spectra of alkali silicate glasses and corresponding crystals and on normal-mode calculations of small molecularlike silicate units using valence-type potentials.^{25–31}

Therefore in the present paper we present realistic VDOS and Raman intensity calculations of Na₂Si₄O₉ glass (denoted hereafter NS4) and discuss the character of the vibrational modes in depolymerized alkali silicate glasses in comparison with amorphous SiO₂. We have chosen the NS4 composition because it can serve as a simple model for more complicated multicomponent high-silica glasses and its structure as well as vibrational spectra have been studied by neutron diffraction,^{32,33} reverse Monte Carlo simulations,³⁴ and Raman and nuclear magnetic resonance (NMR) spectroscopy.^{27,28,35–43}

The outline of the paper is as follows. In Sec. II we discuss the calculation of VDOS by direct diagonalization of the dynamic matrix and of the polarized Raman spectra using the bond polarizability approximation. In order to determine a transferable set of force constants and bond polarizability parameters we have also presented in Sec. II lattice dynamics and Raman intensity calculations of several crystalline SiO₂ polymorphs and crystalline Na₂SiO₃. In Sec. III we describe briefly the construction of an *a*-SiO₂ model by molecular dynamics and two NS4 models. The first model is constructed by molecular dynamics and the second by reverse Monte Carlo simulations. In Sec. IV the vibrational density of states, the character of the vibrational modes, as well as the total and partial Raman spectra of the NS4 and *a*-SiO₂ glass models are compared and discussed. Section V gives a conclusion.

II. CALCULATION PROCEDURES

A. Calculation of normal modes

A large number of interatomic potentials have been used to reproduce the structure, the elastic, and vibrational properties of *a*-SiO₂ and silicate glasses (see for review Refs. 4 and 7). Comparison^{7,8} of the experimentally measured VDOS for *a*-SiO₂ by neutron inelastic scattering with calculated VDOS using several pair potentials indicated that the van Beest, Kramer, and van Santen⁴⁴ potential gives the best overall agreement, followed by the Tsuneyuki *et al.*⁴⁵ potential. However, none of these potentials can reproduce correctly the shape of the low-frequency peak in VDOS at about 360–403 cm⁻¹. VDOS derived from the velocity-velocity autocorrelation function^{4,9} using empirical potentials with both two-body and three-body interactions^{46,47,65} also have this low-frequency deficiency probably due to insufficient dispersion.¹³ *Ab initio* calculations⁵ give the best agreement with the experimental VDOS for *a*-SiO₂ but at present are limited to relatively small structural models.

The large number of available interatomic potential functions for silicate glasses arises from the difficulties to model the strong directional character of the Si-O covalent interactions, especially the bending modes of the coupled SiO₄ units, and leads to rather large uncertainty in the numerical values of the various force constants and in their transferability to other compositions.

Therefore in the present work we have used a Kirkwood-type potential, which, similarly to the Keating potential, is specially suited for the vibrational analysis of covalently bonded materials in the harmonic approximation. The Kirkwood potential can be written in the form

$$2V = \sum_{ij} \alpha_{ij} (r_{ij} - r_{ij}^0)^2 + \sum_{ijk} \beta_{ijk} r_{ij}^0 r_{jk}^0 (\Delta \Theta_{ijk})^2, \quad (1)$$

$$\Delta \Theta_{ijk} = \cos(\Theta_{ijk}) - \cos(\Theta_{ijk}^0),$$

where α_{ij} is the stretching force constant between nearest-neighbors atoms i and j , r_{ij} and r_{ij}^0 are the distance and the equilibrium distance between atoms i and j , β_{ijk} is the bending force constant between the atoms i , j , and k , forming the angle Θ_{ijk} , and Θ_{ijk}^0 is the equilibrium angle between atoms i - j - k with the j th atom at the vertex. In this definition the force constants α and β have the same dimension (N/m).

We calculate the atomic vibrations of the relaxed models by direct diagonalization of the dynamical matrix (DM) using the Jacobi method. Because of the special form of the Kirkwood potential, the DM can be split into purely stretching and purely bending parts:

$$DM_{ij\alpha\beta} = \frac{1}{(m_i m_j)^{1/2}} \frac{\partial^2 V}{\partial r_{i\alpha} \partial r_{j\beta}} = DM_{ij\alpha\beta}^{\text{str}} + DM_{ij\alpha\beta}^b, \quad (2)$$

where i, j number the atoms ($i, j = 1, 2, \dots, N$, N is the total number of atoms in the model), α and β are the Cartesian coordinate indices, m_i is the mass of the atom i , and $r_{i\alpha}$ is the α th component of the radius vector of the i th atom. Detailed expressions for DM^{str} and DM^b are given elsewhere.^{28,48}

B. Raman scattering mechanisms

The one-phonon Raman scattering, in a semiclassical treatment, is associated with the induced polarizability of the system α which relates the induced dipole moment \mathbf{P} to the electric vector of the incident light \mathbf{E} ($\mathbf{P} = \alpha \mathbf{E}$). The intensity of the scattered light is proportional to the space average of the squares of the vibrational transition probabilities $(\alpha_{ij})_{fi} = \langle \Psi_{vf} | \alpha_{ij} | \Psi_{vi} \rangle$, where Ψ_{vf} and Ψ_{vi} are the time independent vibrational wave functions of the final and initial states. Expanding the polarizability tensor in terms of the atomic displacements for a given normal mode p and keeping only the linear term the induced polarizability tensor of the p th vibrational mode becomes

$$\alpha_{ij}^p = \sum_l \frac{\partial \alpha_{ij}^p}{\partial u_l^p} u_l^p, \quad (3)$$

where u_l^p is the displacement of atom l in mode p and the summation is over all atoms in the model. Introducing Eq. (3) into the vibrational transition probability, space averaging the squares of the polarizability tensor components and taking into account the properties of the harmonic vibrational wave functions (see Ref. 49), one obtains for the intensity of a given mode p with polarizability ij :

$$I_{ij}^p \propto \frac{(\omega_0 - \omega_p)^4}{\omega_p} (\alpha_{ij})_p^2 n(\omega_p, T) g(\omega_p), \quad (4)$$

where ω_0 is the wave number of the incident light, $n(\omega_p, T) = [\exp(hc\omega_p/kT) - 1]^{-1}$ is the phonon occupation number at temperature T for the Stokes lines, h is the Planck's constant, c is the speed of light in vacuum, k is the Boltzmann's constant, and $g(\omega_p)$ is the partial vibrational density of states for mode p at frequency ω_p (expressed in wave numbers).

The Raman spectra of disordered solids are usually discussed in terms of the so-called reduced spectrum I^{red} , which is obtained by multiplying the experimentally measured spectrum with the correction factor $\omega/n(\omega, T) \cdot (\omega_0 - \omega)^4$. The importance of the total reduced (*temperature-independent*) scattering is due to the fact that it can be written as a sum over all partial vibrational densities of states.^{18,19}

$$I^{\text{red}} = \sum_p C_p^\alpha g_p(\omega), \quad (5)$$

where the coupling coefficients C_p^α between the partial density of states and the optical spectrum for a given polarization α are proportional to the space averages of the squares of the derivative α' of the polarizability tensor.

For an isotropic system there are only two independent components of the α_{ij} tensor—VV and VH. The polarization of the experiment is VV when the incident and the scattered electric fields are parallel and is VH when they are perpendicular. It can be shown⁴⁹ that the reduced intensities of mode p with polarizations VV and VH will be

$$I_{\text{VV}}^{\text{red}} \propto (45T_p^2 + 4G_p^2)g(\omega_p) \quad (6)$$

and

$$I_{\text{VH}}^{\text{red}} \propto 3G_p^2g(\omega_p), \quad (7)$$

where T_p and G_p^2 are the invariants of the induced polarizability tensor α when the system is vibrating in mode p :

$$T_p = \frac{1}{3}(\alpha_{11}^p + \alpha_{22}^p + \alpha_{33}^p) \quad (8)$$

and

$$G_p^2 = \frac{1}{2}[(\alpha_{11}^p - \alpha_{22}^p)^2 + (\alpha_{11}^p - \alpha_{33}^p)^2 + (\alpha_{22}^p - \alpha_{33}^p)^2] + 3[(\alpha_{12}^p)^2 + (\alpha_{13}^p)^2 + (\alpha_{23}^p)^2]. \quad (9)$$

In order to evaluate the Raman intensities from Eqs. (6) and (7) we have used the bond polarizability approximation,^{22,50} in which all six components α_{ij} of the induced polarizability tensor are written as a sum over the nearest-neighbor bonds with imposed invariance with respect to translation and inversion and cylindrical symmetry about the bond. The contribution from the bond between atoms a and b will be then

$$\alpha_{ij}(\mathbf{R}_{ab}) = A(R_{ab})\delta_{ij} + \gamma(R_{ab})(\hat{r}_{ab}\hat{r}_{ab} - 1)_{ij}, \quad (10)$$

where $\mathbf{R}_{ab} = \mathbf{r}_a - \mathbf{r}_b$ is the vector joining atoms a and b , R_{ab} is the bond length, \hat{r}_{ab} is a unit vector along the bond, and $A(R_{ab})$ and $\gamma(R_{ab})$ are the parallel and perpendicular bond

TABLE I. Symmetry properties of the Raman scattering tensors.

Mechanism	T^a	G^b	ρ^c
1	finite	0	0
2	0	finite	$\frac{3}{4}$
3	0	finite	$\frac{3}{4}$

$$^a T = \frac{1}{3}(\alpha_{11} + \alpha_{22} + \alpha_{33}).$$

$$^b G^2 = \frac{1}{2}[(\alpha_{11} - \alpha_{22})^2 + (\alpha_{11} - \alpha_{33})^2 + (\alpha_{22} - \alpha_{33})^2] + 3[(\alpha_{12})^2 + (\alpha_{13})^2 + (\alpha_{23})^2].$$

^cDepolarization ratio.

polarizability parameters. Expanding $\alpha_{ij}(R_{ab})$ in a Taylor series and keeping the linear term only, Eq. (3) obtains the form

$$\alpha_{ij}^p = \sum_m A'_m \Delta u_m^p \cdot \hat{r}_{ab} \delta_{ij} + \sum_m \gamma'_m \Delta u_m^p \cdot \hat{r}_{ab} (\hat{r}_{ab} \hat{r}_{ab} - 1)_{ij} + \sum_m \frac{\gamma_m}{R_{ab}} (\Delta u_m^p \hat{r}_{ab} + \hat{r}_{ab} \Delta u_m^p - 2 \Delta u_m^p \cdot \hat{r}_{ab} \hat{r}_{ab} \hat{r}_{ab})_{ij}, \quad (11)$$

where A'_m and γ'_m are the derivatives of A and γ with respect to R_{ab} , $\Delta u_m^p = \mathbf{u}_a^p - \mathbf{u}_b^p$, and the summations are over all nearest-neighbor bonds. Assuming further that the parallel and perpendicular bond polarizabilities vary slowly with the bond length for a given type of bonds, we can rewrite Eq. (11) in the form

$$\alpha_{ij}^p = \sum_n \bar{A}'_n \sum_m \Delta u_m^p \cdot \hat{r}_{ab} \delta_{ij} + \sum_n \bar{\gamma}'_n \sum_m \Delta u_m^p \cdot \hat{r}_{ab} (\hat{r}_{ab} \hat{r}_{ab} - 1)_{ij} + \sum_n \bar{\gamma}_n \sum_m \frac{1}{R_{ab}} (\Delta u_m^p \hat{r}_{ab} + \hat{r}_{ab} \Delta u_m^p - 2 \Delta u_m^p \cdot \hat{r}_{ab} \hat{r}_{ab} \hat{r}_{ab})_{ij}, \quad (12)$$

where n runs over the different types of bonds and m is a summation over all bonds of type n , \bar{A}'_n , $\bar{\gamma}_n$, and $\bar{\gamma}'_n$ are the *mean* bond polarizability parameters for the n th type of bonds. The three terms in the right-hand side of Eq. (12) correspond to three different types of Raman-scattering mechanisms. The symmetry of the invariants of the three polarizability tensors are summarized in Table I. The first term ($45T_p^2$) in the VV polarized spectrum [Eq. (6)] depends only on the first scattering mechanism, the polarizability tensor of which is diagonal and corresponds to bond compression. On the contrary, the depolarized VH Raman scattering [Eq. (7)] depends only on traceless mechanisms 2 and 3, which correspond to mixed bond-stretching and bond-bending motions.

Although the mean polarizability parameters can be estimated in simple cases,⁵¹ we will consider them as free parameters which must be adjusted to give a best fit to the experimental Raman intensities. A similar approach was adopted by Murray and Ching.³

The final Raman spectra to be compared with experimentally measured reduced spectra are obtained by uniform Gaussian broadening of the calculated Raman intensities which takes into account the effects of anharmonicity, finite

size of the models, and additional disorder not present in the computer generated models. The consequences of this line-broadening procedure for the calculated Raman spectra will be discussed in Sec. IV.

C. Fit of force constants and bond polarizability parameters

We have determined the force constants of the Kirkwood potential from lattice dynamics calculations on several crystalline SiO_2 polymorphs and crystalline Na_2SiO_3 metasilicate, the structure and the vibrational (Raman and IR) spectra of which are well established. The symmetry species of the modes are determined in each case by analyzing the transformation properties of the eigenvectors. While the irreducible representations of the optic phonons Γ_{opt} for the SiO_2 polymorphs are well known, we have calculated Γ_{opt} for Na_2SiO_3 using the correlation method⁵² (see Table III below). The calculated phonon frequencies and relative intensities were fitted to the experimentally measured frequencies and intensities reported in the literature,^{27,53–61} except for α quartz the intensities of which were determined from unpolarized Raman measurements in the present study. In the lattice dynamics calculations we have not included force constants for bending of Na-O-Si and O-Na-O linkages because they are expected to be very small.

Examples of the lattice dynamics and Raman intensity calculations for α quartz and Na_2SiO_3 are given in Tables II and III, respectively. Despite the relatively simple form of the Kirkwood potential, it correctly reproduces the number and the symmetry of the vibrational modes. It does not predict the LO-TO splittings in α quartz and α cristobalite, because Coulomb and dipole-dipole interactions are not included in the potential model.

Table IV lists the values of the force constants for all crystalline phases studied. A reasonably good fit is achieved for all phases, except for β cristobalite which has only three (one Raman and two IR) optical active phonons, to which the force constants can be fitted. The valence force constants for β quartz are in excellent agreement with previous calculations by Bates.⁶² All SiO_2 polymorphs can be fitted with one single set of average force constants $\langle\alpha_{\text{Si-BO}}\rangle=476 \pm 14$ N/m, $\langle\beta_{\text{BO-Si-BO}}\rangle=39 \pm 15$ N/m, and $\langle\beta_{\text{Si-BO-Si}}\rangle=3.4 \pm 2.4$ N/m. This demonstrates the transferability of the empirical Kirkwood force constants for different SiO_2 polymorphs.

The intensities calculated by mechanisms 2 and 3 are strongly correlated. Therefore we have set the value of the derivative of the perpendicular bond polarizability $\bar{\gamma}'$ to zero in all calculations. In other words we assume that the perpendicular bond polarizability γ does not depend on the bond length. The relative intensities for the SiO_2 polymorphs are reasonably well reproduced with an average $\bar{\gamma}/\bar{A}'$ ratio of about 0.1, except of the lowest frequency modes in α quartz, α cristobalite, and coesite which are systematically lower. This might be due to the presence of significant torsional component⁶² in these modes, which is not included in the potential model. The ratio $\bar{\gamma}/\bar{A}'=0.1$ is comparable to the value 0.3 used by Murray and Ching.³ For the sodium metasilicate the calculations reproduce the relative order of the Raman intensities (see Table III) with the following set of

TABLE II. Observed and calculated frequencies (cm^{-1}) and relative integral intensities of Raman-active optic phonons in α quartz. $\Gamma_{\text{opt}}=4A_1(R)+4A_2(I)+8E(R,I)$.

Symmetry ^a	Frequencies			Assignment ^d	Intensities	
	Raman ^b	IR ^c	Calc.		Obs. ^e	Calc.
$E(T+L)$	128	129	103	E	6.3	0.26
A_1	206		189	A_1	35	24
$E(T+L)$	265	266	232	E	3.8	0.3
A_1	355		316	A_1	4.0	9.44
A_2		364	297	A_2		0.0
$E(T)$	394	385			1.8	
			400	E		0.5
$E(L)$	401				1.5	
A_1	464		464	A_1	100	100
A_2		495	405	A_2		0.0
$E(T)$	450	444			sh ^f	
			340	E		0.04
$E(L)$	511				1.3	
$E(T+L)$	696	689	642	E	2.1	0.9
A_2		778	730	A_2		0.0
$E(T)$	796	800			2.5	
			778	E		2.7
$E(L)$	808				2.5	
$E(T)$	1069				1.8	
			1041	E		0.8
$E(L)$	1230				1.0	
A_2		1110	1160	A_2		0.0
A_1	1085		1152	A_1	1.9	0.3
$E(T+L)$	1162		1157	E	6.0	0.3

^aSymmetry species from single-crystal Raman measurements (Ref. 53).

^bScott and Porto (Ref. 53).

^cScott and Porto (Ref. 53), Plendl *et al.* (Ref. 54).

^dSymmetry assignment from the transformation properties of the calculated normal modes.

^eUnpolarized powder Raman measurement in the present study.

^fShoulder.

parameters: $\bar{\gamma}_{\text{Si-BO}}=0.05$, $\bar{A}'_{\text{Si-BO}}=0.5$, $\bar{\gamma}_{\text{Si-NBO}}=0.05$, $\bar{A}'_{\text{Si-NBO}}=1$, $\bar{\gamma}_{\text{Na-O}}=0.0$, and $\bar{A}'_{\text{Na-O}}=0.05$.

The results for the SiO_2 polymorphs and crystalline Na_2SiO_3 demonstrate that lattice dynamics calculations with the Kirkwood potential and Raman-scattering intensities based on the mean bond polarizability approximation can reproduce correctly the main features of the corresponding vibrational spectra and thus could be used for the vibrational analysis of silicate glasses which have similar short-range order.

III. CONSTRUCTION OF GLASS MODELS

A. SiO_2 model

A model of a - SiO_2 was constructed by molecular-dynamics (MD) simulations. The MD calculations were performed with an interatomic potential including two- and three-body interactions, described in detail by Vashishta *et al.*⁴⁷ The model contains 648 atoms (216 Si atoms and 432

TABLE III. Calculated and observed frequencies (cm^{-1}) and relative intensities of Raman-active optic phonons in crystalline Na_2SiO_3 . $\Gamma_{\text{opt}}=9A_1(R,I)+8A_2(R)+7B_1(R,I)+9B_2(R,I)$.

Experiment				Calculation		
Freq. ^a	Int. ^a	Freq. ^b	Int. ^{b,c}	Freq. ^d	Int.	Assignment ^e
168	m ^c	167	3	174	1.0	B_2
184	w	185	3	186	1.3	A_1
200	w					
215	w	215	1	201	4.8	B_1
235	sh	235	2	253	1.5	A_2
264	m	263	2	259	3.4	A_1
301	w	303	2	296	0.4	B_2
				355	0.5	A_2
395	m	397	5	411	5.4	A_1
433	vw	407	sh	383	0.2	B_1
510	w	507	1	507	0.9	B_2
549	w	553	1			
588	s	587	18	583	18	A_1
607	sh					
716	vw					
750	vw			816	<.1	B_2
865	w	880	3	767	1.6	B_2
914	vw					
965	vs	973	100	971	100	A_1
1014	vw	1018	9	1018	1.7	A_1
				1063	<0.1	B_2
1063	w	1083	3	1101	0.3	A_2
				1103	0.1	B_1

^aReference 61

^bReference 27.

^cvw: very weak; w: weak; m: medium; sh: shoulder; s: strong; vs: very strong intensity. Approximate reduced intensities ($T=298\text{ K}$) calculated in the present study from the height of the peaks given in Fig. 1 of Ref. 27.

^dThe first 15 normal mode with frequencies below 30 cm^{-1} , involving mainly Na-O motion, are not listed.

^eSymmetry assignment on the basis of the transformation properties of the calculated normal modes and the relative Raman intensities.

oxygen atoms) with periodic boundary conditions (see Table V). The equations of motion were integrated with an algorithm due to Beeman and Alben⁶³ using a time step of 0.5 fs. The scheme of the cooling and thermalization procedures for generating the glass at RT from a well thermalized molten state is the same as described by Vashishta *et al.*⁴⁷

TABLE IV. Fitted force constants (in N/m) for SiO_2 crystalline polymorphs and Na_2SiO_3 .

Phase	$\alpha_{\text{Si-BO}}$	$\alpha_{\text{Si-NBO}}$	$\beta_{\text{O-Si-O}}$	$\beta_{\text{Si-O-Si}}$	$\alpha_{\text{Na-O}}$
α quartz	480	-	25.0	2.5	-
β quartz	490	-	20.5	3.8	-
α cristobalite	460	-	39.0	4.0	-
β cristobalite	475	-	41.5	6.5	-
coesite	475	-	41.5	6.5	-
Na_2SiO_3	383	603	35.0	23	0.5

B. $\text{Na}_2\text{Si}_4\text{O}_9$ models

Models of $\text{Na}_2\text{Si}_4\text{O}_9$ glass were constructed using two different procedures. The first model (denoted NS4_I hereafter) was generated by molecular dynamics. The MD calculations were carried out with constant particle number and constant pressure. The particle velocities and positions, as well as the dimensions of the simulation cell, were slightly rescaled at each time step in order to control the systems temperature and pressure. The Newtonian equations of motion were integrated with an integration step of 1 fs using the Nordsieck-Gear algorithm.⁶⁴ The simulation started with a stoichiometrically modified crystalline structure. In 500-ps annealing cycle this structure was rapidly heated up to a maximum temperature of $T=8000\text{ K}$ and subsequently slowly cooled down to room temperature. The MD calculation is based on a modified Born-Mayer-Huggins potential for ionic interactions with a weak Stillinger-Weber three-body term.⁶⁵ Further details of the MD calculations are given elsewhere.^{66,67} The model contains 585 atoms (156 Si, 281 BO, 70 NBO, and 78 Na atoms) in a box with periodic boundary conditions. The number density (see Table V) is very close to the experimental value of $0.0714\text{ atoms}/\text{\AA}^3$.

The second model (denoted NS4_II hereafter) was constructed in several steps. We started with a 64-atom model of α -Si, generated by the recently proposed activation-relaxation technique.⁶⁸ Oxygen atoms were then inserted into the middle of all Si-Si bonds. As a next step some of the Si-O-Si linkages were broken and additional NBO's added close to the Si atoms to have approximately the correct number of Q species in the NS4 glass, as determined from NMR measurements.⁴⁰⁻⁴³ Finally Na atoms were added in the voids of the Si-O network and a reverse Monte Carlo (RMC) fit of the calculated pair correlation function $g(r)$ to the experimentally measured $g(r)$ using neutron-diffraction³² data was performed. The configuration created in this way contained 234 atoms (62 Si, 142 O, and 30 Na atoms) in a cubic box with periodic boundary conditions. The number density (see Table V) is slightly lower than the experimental one.

C. Energy relaxation

The initial models were then relaxed with the Kirkwood potential. The values of the valence force constants for α - SiO_2 were chosen close to the force constants given in Table IV: $\alpha_{\text{Si-BO}}=480\text{ N/m}$, $\beta_{\text{BO-Si-BO}}=40\text{ N/m}$, and $\beta_{\text{Si-BO-Si}}=5\text{ N/m}$. The values used for relaxation of the NS4 models were $\alpha_{\text{Si-BO}}=465\text{ N/m}$, $\beta_{\text{O-Si-O}}=35\text{ N/m}$, $\beta_{\text{Si-BO-Si}}=10\text{ N/m}$, $\alpha_{\text{Si-NBO}}=655\text{ N/m}$, and $\alpha_{\text{Na-O}}=0.6\text{ N/m}$.

The equilibrium O-Si-O bond angle in all cases was set equal to the ideal tetrahedral value of 109.47° . The equilibrium Si-NBO bond length was chosen equal to 1.59 \AA in agreement with our previous RMC simulations³⁴ and the measured Si-NBO bond length in crystalline sodium silicates.^{69,70} The equilibrium Si-BO, Na-BO, and Na-NBO bond lengths as well as the equilibrium Si-O-Si bond angles are given in Table V. The value $\epsilon_0=144^\circ$ for the α - SiO_2 model is the same as proposed by Mozzi and Warren⁷¹ and Gaskell and Tarrant.⁷²

The minimization of the strain energy was achieved iteratively. The force on each atom was calculated, which was then moved in a direction that decreases the force acting on it

TABLE V. Structural characteristics of the relaxed SiO_2 and $\text{Na}_2\text{Si}_4\text{O}_9$ glass models.

	SiO_2 model	NS4_I model	NS4_II model
No. of atoms	648	585	234
Box edges, Å	21.41	19.87; 21.11; 19.19	15.21
Density, atoms/Å ³	0.0662	0.0727	0.06654
$r_0(\text{Si-BO})$, Å	1.62	1.625	1.657
$r_0(\text{Na-BO})$, Å	-	2.74	2.70
$r_0(\text{Na-NBO})$, Å	-	2.53	2.59
ϵ_0 , deg	144	149	149
$\langle r(\text{Si-BO}) \rangle$, Å	1.643 ± 0.015	1.628 ± 0.016	1.66 ± 0.26
$\langle r(\text{Si-NBO}) \rangle$, Å	-	1.59 ± 0.01	1.59 ± 0.02
$\langle r(\text{Na-BO}) \rangle$, Å	-	2.73 ± 0.12	2.71 ± 0.13
$\langle r(\text{Na-NBO}) \rangle$, Å	-	2.53 ± 0.13	2.58 ± 0.18
$CN(\text{Si})^c$	3.94 ± 0.22	4.05 ± 0.22	3.9 ± 0.46
$CN(\text{Na})$	-	4.96 ± 1.1	5.2 ± 1.3
$CN(\text{O})$	1.97 ± 0.18	1.8 ± 0.4	1.7 ± 0.5
$\langle \tau(\text{O-Si-O}) \rangle$, deg	109.4	109.4	109.4
FWHM (O-Si-O)	3.0	3.0	4.3
$\langle \epsilon(\text{Si-O-Si}) \rangle$, deg	144	150	149
FWHM (Si-O-Si)	24.4	20.7	21.5
Q^1 , %	0	0	4.8
Q^2 , %	1.8	7.7	6.4
Q^3 , %	9.2	28.2	50.0
Q^4 , %	89.0	60.2	38.8
$R3^a$	10	6	0
$R4$	20	35	1
$R5$	83	56	4
$R6$	111	60	35
$\langle \Delta \rangle$, Å ^b	0.13 ± 0.09	0.16 ± 0.13	0.48 ± 0.29

^a $R3$: three membered; $R4$: four membered, $R5$: five membered; and $R6$: six membered rings.

^bAverage shift of the atoms in the relaxed models.

^cCN: coordination number.

without allowing bond breaking or reconstruction. This process is repeated until convergence is achieved (typically after about 20–60 iterations).

The structural characteristics of the relaxed models are given in Table V. The comparison of the peak positions of the calculated (Fig. 1) and experimental radial distribution functions^{32,71,73,74} as well as the corresponding average coordination numbers demonstrate that the relaxed SiO_2 and NS4 models are consistent with the available x-ray and neutron-scattering data. The α - SiO_2 model contains a significant number of five- and six-membered rings. The ring distribution in α - SiO_2 has been a matter of controversy for quite some time especially in connection with the possible origin of the D_1 and D_2 “defect” lines at about 495 and 606 cm^{-1} in the polarized Raman spectrum from planar four- and three-membered rings (see Galeener⁷⁵ and references therein). In fact, recent analysis of the VDOS of an α - SiO_2 model obtained by quantum MD simulations have demonstrated⁷⁶ that the partial VDOS of the three- and four-membered rings in this model yield peaks at frequencies in very good agreement with the Raman data. But since the VDOS and the polarized Raman spectra of α - SiO_2 in the present study serve mainly as a reference in analysis of the vibrational properties of depolymerized glasses we will not discuss this question in further detail.

The main difference between the two NS4 models is in the medium-range order (the ring distribution) and the Q speciation. The NS4_I model has significant number of four-, five-, and six-membered rings while only six-membered rings dominate the structure of the NS4_II model. Although both models have composition close to the ideal stoichiometric formula $\text{Na}_2\text{Si}_4\text{O}_9$, the Q species in both NS4 models (see Table V) slightly deviate from the experimentally observed^{40–43} Q species distribution of about 2% Q^2 , 50% Q^3 , and 48% Q^4 . We use these relaxed models in the next section to investigate the character of the vibrational modes with increasing degree of depolymerization ($\propto 0\%$ Q^3 in α - SiO_2 , 28% Q^3 in NS4_I, and 50% Q^3 in NS4_II).

IV. RESULTS AND DISCUSSION

A. Vibrational density of states

The vibrational densities of states (VDOS), scaled to one and the same number of Si atoms, are plotted in Fig. 2. The calculated VDOS for α - SiO_2 is usually compared with the experimentally measured inelastic neutron scattering (INS) spectrum $G(Q, \omega)$.^{77,78} No INS spectra for sodium silicate glasses exist to the best of our knowledge.

The calculated VDOS for α - SiO_2 (Fig. 2) is in relatively good agreement with the experimental $G(Q, \omega)$ and compa-

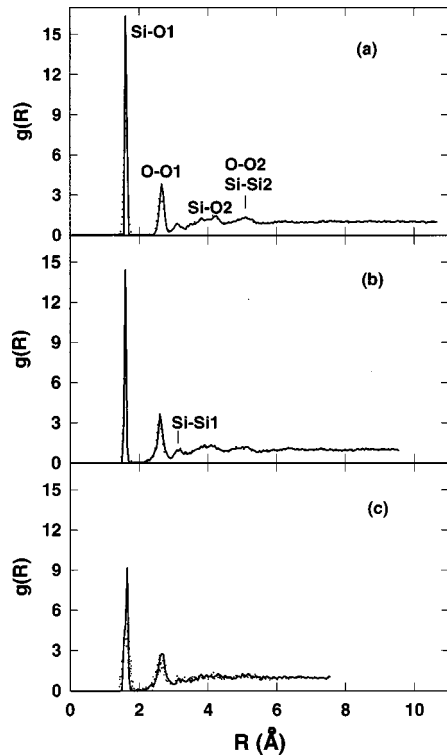


FIG. 1. Pair correlation functions $g(r)$ of the unrelaxed (dotted lines) and the relaxed (full lines) models: (a) a -SiO₂; (b) NS4_I; (c) NS4_II model. The first- and second-nearest-neighbor peaks in $g(r)$ are labeled.

rable with other VDOS calculations for a -SiO₂.^{1,2-10,13-15} In particular, the calculations reproduce well the shape and the position of the low-frequency band observed at about 403 cm⁻¹, the mid-frequency band observed at 795 cm⁻¹, and the high-frequency bands which in the experimental $G(Q, \omega)$ are at about 1060 and 1190 cm⁻¹, respectively.^{77,78} However, the the high-frequency band splitting is smaller and the intensity of the mid- and high-frequency bands is enhanced compared to the intensity of the low-frequency band. It is

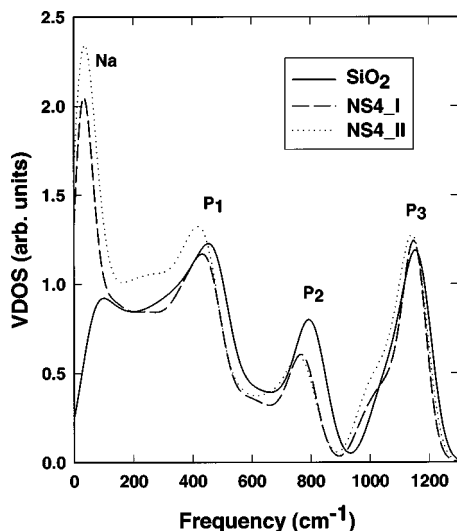


FIG. 2. Vibrational density of states: (—) a -SiO₂; (----) NS4_I; (· · · ·) NS4_II model. The letters label the main peaks in VDOS.

interesting to note that all VDOS calculations except the Bell and Dean model,¹ the Bethe lattice model,^{14,15} both of which use Born potential, and the *ab initio* MD constructed model⁵ have this intensity deficiency.

Introduction of Na₂O into the SiO₂ glass has several effects on the VDOS. A new strong peak at about 35 cm⁻¹ appears which is due to the correlated motion of the Na atoms (see below). The increase of the intensity of the high-frequency peak at about 1000 cm⁻¹, the significant loss of intensity of the mid-frequency peak at about 800 cm⁻¹, and the intensity increase in the 200–400-cm⁻¹ range correlate with the degree of depolymerization and thus are associated with the presence of nonbridging oxygens.

B. Character of the vibrational modes

Unlike crystals, the vibrational modes of a glass cannot be classified according to the irreducible representations of the corresponding space group of symmetry. Nevertheless, it is possible to separate out different aspects of the vibrational modes by making use of the local symmetry of the atomic arrangements.

1. Localization

An overall measure of the localization of the normal modes is the so-called participation ratio p_c , introduced by Bell, Dean, and Hibbins-Butler:⁷⁹

$$p_c(\omega_p) = \frac{(M_1)^2}{M_0 M_2}, \quad (13)$$

where $M_n = \sum |u_p^i|^{2n}$ and the summation is over all atoms in the model. If the mode p is delocalized and all atoms vibrate with approximately the same amplitudes, p_c will be close to +1. If on the contrary, the mode p is strongly localized on a given atom, then $p_c \rightarrow 1/N$.

The participation ratio $p_c(\omega)$ for the a -SiO₂ and NS4 models is shown in Fig. 3. The general character of $p_c(\omega)$ for all three models is similar despite the different degree of polymerization. Two types of modes are observed: (i) almost fully delocalized modes with $p_c \sim 0.47$ for the a -SiO₂ model and $p_c \sim 0.35$ in the NS4 models and (ii) localized modes for which p_c is much lower. The delocalized modes in the SiO₂ model of Taraskin and Elliott⁷ also have p_c of about 0.5 which might be taken as characteristic for a -SiO₂. In general, the participation ratio becomes smaller with increasing size of the models.⁷⁹ The fact that p_c is larger for the a -SiO₂ model, although it has the largest number of atoms, shows that depolymerization leads to decrease of the localization, especially of the low- and mid-frequency modes.

The localized modes are grouped around specific frequencies: 50–100 (in the NS4 glass), 250–350, 500, 610, 720, 850, 980, 1100, and 1210 cm⁻¹ shown with dashed lines in Fig. 3. Comparison of these frequencies with the position of the main peaks in VDOS shows that for both the a -SiO₂ and the NS4 models most of the localized modes are grouped near *band edges*. Thus we confirm with much better statistics a similar observation by Bell, Bird, and Dean¹ for a -SiO₂.

Using the participation ratio we can thus separate the VDOS bands into eight frequency ranges (bands): 0–100 cm⁻¹ (Na band), 100–350 cm⁻¹ (B_1 band), 350–500 cm⁻¹

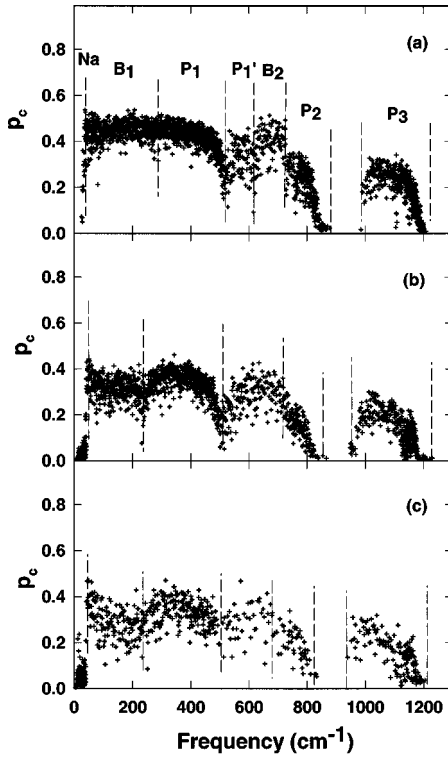


FIG. 3. Participation ratio: (a) a -SiO₂; (b) NS4_I; (c) NS4_II model. The dashed vertical lines mark the position of the band edges. The letters label the bands in VDOS.

(P_1 band), 500–610 cm⁻¹ (P'_1 band), 610–720 cm⁻¹ (B_2 band), 720–850 cm⁻¹ (P_2 band), and finally 950–1210 cm⁻¹ (P_3 band). The width of the vibrational gap 850–950 cm⁻¹ remains practically unchanged with increasing depolymerization, but the separation between the P'_1 , B_2 , and P_2 bands becomes more smeared out.

Although our calculations of VDOS involve significant noncentral forces it is interesting to compare the results so far with the predictions of the central-force model of Sen and Thorpe^{16,17} augmented by Galeener, Leadbetter, and Stringfellow⁷⁷ with rocking motions and acoustic modes [augmented central force (ACF) model], which has provided important insights into the vibrational dynamics of SiO₂, GeO₂, and BeF₂ glasses. The relative weights of the B_1 , P_1 , $P'_1+B_2+P_2$, and the P_3 bands, which correspond to the division of Galeener, Leadbetter, and Stringfellow,⁷⁷ are 3.4/9, 1.7/9, 2.1/9, and 1.8/9, in close agreement with the predictions of the ACF model (3/9, 2/9, 2/9, and 2/9). It should be pointed out, however, that the ACF model has taken only *approximately* into account the nearest-neighbor noncentral forces.

The separation of the VDOS of a -SiO₂ and NS4 glasses into eight bands is supported by all vibrational characteristics given below, which always have some kind of *singularity* (minimum, maximum, steps, inflection points, etc.) near the corresponding band edges.

2. Stretching character

The stretching character S describes the extent to which a given mode is stretching or bending:

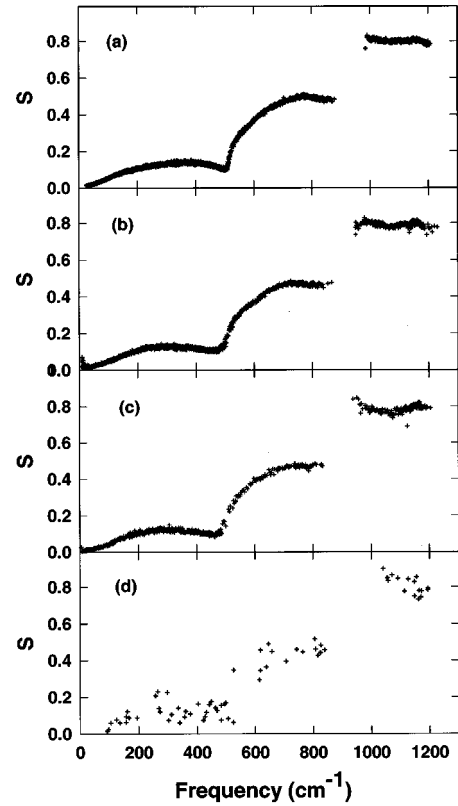


FIG. 4. Stretching character of the vibrational modes: (a) a -SiO₂; (b) NS4_I; (c) NS4_II model; (d) coesite.

$$S(\omega_p) = \frac{\sum |(u_p^i - u_p^j) \cdot \hat{r}_{ij}|}{\sum |u_p^i - u_p^j|}, \quad (14)$$

where the symbols are as defined in Eqs. (3) and (10). The value of S will be close to +1 if mode p is predominantly of bond-stretching (compressing) type and close to 0 if mode p is predominantly of bond-bending type.

The stretching character (S) of the models studied as well as for coesite is plotted in Fig. 4. We can distinguish three regions: 0–500, 500–850, and 980–1210 cm⁻¹. The low-frequency range, which comprises the (Na), B_1 , and P_1 bands, is of predominantly bending character with $S \leq 0.17$. The mid-frequency range, which comprises the P'_1 , B_2 , and P_2 bands, has mixed bending+stretching character ($0.17 \leq S \leq 0.6$) with the stretching contribution increasing with frequency. The high-frequency range, which coincides with the P_3 band, is almost purely stretching in character ($S \geq 0.8$). Comparison of the stretching character of the different models and coesite shows that the depolymerization and disorder have hardly effect on the stretching-bending character of the vibrational modes.

3. Bridging oxygen motion

The vibrations of the bridging oxygens (BO) may be classified as stretching (S_{BO}), bending (B_{BO}), or rocking (R_{BO})⁸⁰ according to whether *locally* the BO atoms move parallel to the line joining the two Si neighbors, parallel to the bisector of the Si-O-Si angle or the motion is perpendicular to the Si-O-Si plane, respectively. We define the parameters S_{BO} , B_{BO} , and R_{BO} in the following way:

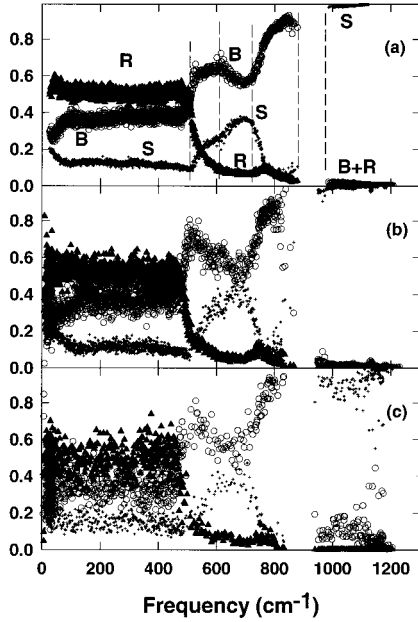


FIG. 5. Bridging oxygen stretching (+), bending (O), and rocking (▲) motion: (a) a -SiO₂; (b) NS4_I; (c) NS4_II model. The dashed vertical lines mark the position of the band edges.

$$S_{\text{BO}}(\omega_p) = \frac{\sum_{\text{BO}} u_p^i \cdot \hat{r}_{i-i'}}{\sum_{\text{BO}} |u_p^i|}, \quad (15)$$

$$B_{\text{BO}}(\omega_p) = \frac{\sum_{\text{BO}} u_p^i \cdot \hat{r}_{i+i'}}{\sum_{\text{BO}} |u_p^i|}, \quad (16)$$

and

$$R_{\text{BO}}(\omega_p) = \frac{\sum_{\text{BO}} u_p^i \cdot \hat{r}_{\oplus}}{\sum_{\text{BO}} |u_p^i|}, \quad (17)$$

where \hat{r}_{\oplus} is a unit vector perpendicular to the local Si-O-Si plane, $\hat{r}_{i+i'}$, is a unit vector parallel to the bisector of the Si-O-Si angle and $\hat{r}_{i-i'}$ is a unit vector perpendicular to \hat{r}_{\oplus} and $\hat{r}_{i+i'}$. The summations in Eqs. (15)–(17) are over all bridging oxygens. In this definition S_{BO} , B_{BO} , and R_{BO} all range from +1 for fully stretching, bending or rocking motion to zero and $S_{\text{BO}} + B_{\text{BO}} + R_{\text{BO}} = 1$ for every ω_p . In previous studies^{7,14} the total VDOS of a -SiO₂ was instead decomposed into partial stretching, bending, and rocking components by convolution of S_{BO} , B_{BO} , and R_{BO} with the total VDOS, which in our view smears out the details of the BO motion.

The general character of the bridging oxygen (BO) motion given in Fig. 5 is in very good agreement with the results of Bell, Dean, and Hibbins-Butter,⁸⁰ determined only for selected frequencies of their a -SiO₂ model. The BO motion is strongly frequency dependent. It changes drastically above the 500-cm⁻¹ band edge (R_{BO} decreases, B_{BO} increases), then above the band gap (B_{BO} goes to zero and S_{BO} increases to 1.0) and reveals further details of the fine structure of the P_1' , B_2 , and P_2 bands. The effects of depolymerization on the character of the BO motion are summarized in Table VI.

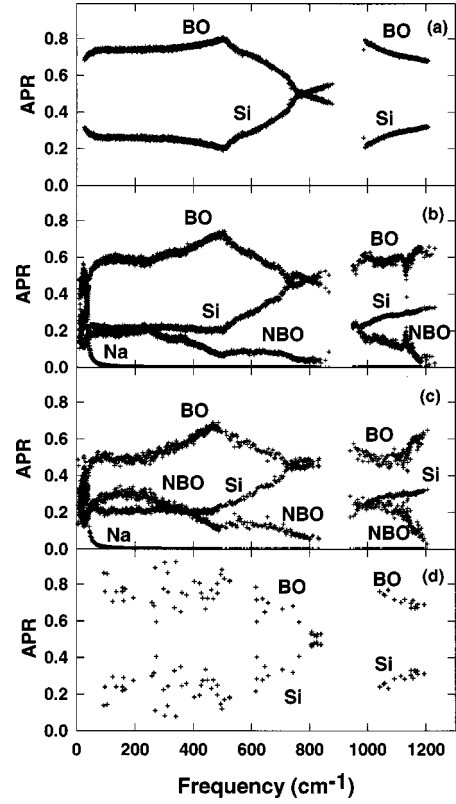


FIG. 6. Atomic participation ratios: (a) a -SiO₂; (b) NS4_I; (c) NS4_II model; (d) coesite.

4. Atomic participation ratios

In order to quantify the contribution of each atom type α to a given normal mode, we introduce the so-called atomic participation ratios (APR_{α})

$$\text{APR}_{\alpha}(\omega_p) = \frac{\sum_{\alpha} |u_p^i|}{\sum |u_p^i|}, \quad \sum_{\alpha} \text{APR}_{\alpha} = 1, \quad (18)$$

where the summation in the nominator is over all atoms of type α and the summation in the denominator is over all atoms in the model. The APR_{α} parameters range from 0, when the α -type atoms do not participate in the p th normal mode, to +1, when only the α -type atoms vibrate.

The frequency dependence of the atomic participation ratios are given in Fig. 6. The atomic contributions change significantly at the band edges. In a -SiO₂ the normal modes below 500 cm⁻¹ involve mainly the BO atoms ($\text{APR}_{\text{BO}} > .7$, $\text{APR}_{\text{Si}} < .3$). In the depolymerized NS4 glasses the Na motion dominates below 100 cm⁻¹, the NBO contribution increases at the expense of the BO contribution, while the Si contribution remains practically unchanged ($\text{APR}_{\text{Si}} \sim 0.22$). Comparing Figs. 5 and 6, it can be seen that the decrease of the BO contribution above 500 cm⁻¹ is mainly due to the strong decrease of the BO rocking motion which cannot be compensated by the small increase of the bending BO motion. The NBO contribution remains at low constant level ($\text{APR}_{\text{NBO}} \propto 0.15$).

Near the 720-cm⁻¹ band edge the Si contribution reaches a maximum while the BO contribution has a minimum, the APR_{NBO} is very low and APR_{Na} is practically zero. Weighted partial VDOS for Si and O (Refs. 4, 7, 14 and 85) in a -SiO₂

TABLE VI. Band assignment and effects of depolymerization on the character of the vibrational modes in alkali silicate glasses.

Band	range (cm ⁻¹)	Phonon type	Assignment		Effect of depolymerization
			Bond type BO type	Main atomic contribution	
Na	0–150	<i>O</i> ^a	<i>S</i> ^b	Na	New band in depolymerized glasses.
<i>B</i> ₁	150–350	<i>A</i>	<i>B</i> (<i>R</i> ₀ + <i>B</i> ₀) ^c	BO+NBO	Formation of new NBO subband at ~300 cm ⁻¹ . Decrease of BO contribution. Increase of the <i>R</i> ₀ and <i>B</i> ₀ mixing.
<i>P</i> ₁	350–500	<i>A</i> + <i>O</i>	<i>B</i> (<i>R</i> ₀ + <i>B</i> ₀)	BO	Decrease of total BO contribution.
<i>P</i> ' ₁	500–610	<i>A</i> + <i>O</i>	<i>B</i> + <i>S</i> (<i>B</i> ₀ + <i>S</i> ₀)	BO	Decrease of total BO concentration. Increase of bending BO contribution. Increase of mode localization.
<i>B</i> ₂	610–720	<i>O</i> + <i>A</i>	<i>B</i> + <i>S</i> (<i>B</i> ₀ + <i>S</i> ₀)	BO+Si	Increase of the stretching BO contribution. Increased mixing of <i>S</i> ₀ and <i>B</i> ₀ motion. Decrease of total BO contribution. Increase of NBO contribution.
<i>P</i> ₂	720–850	<i>O</i>	<i>S</i> + <i>B</i> (<i>B</i> ₀ + <i>S</i> ₀)	Si+BO	Decrease of the total BO contribution. Increase of the bending BO contribution. Slight increase of Si contribution.
<i>P</i> ₃	950–1210	<i>O</i>	<i>S</i> <i>S</i> ₀	BO+Si+NBO	Decrease of total BO contribution. New modes localized on NBO. Increase of the bending BO contribution.

^a*O*: opticlike modes; *A*: acousticlike modes.

^b*S*—stretching type modes, *B*—bending type modes.

^c*R*₀, *B*₀, *S*₀: rocking-, bending-, and stretching-type motion of the bridging oxygen atoms. The order of the symbols from left to right corresponds to the relative weight of the different types of motions.

also show that the peak at about 800 cm⁻¹ is dominated by Si motions against the bridging oxygens.

Above the band gap the NBO contribution sharply increases. Several positive NBO peaks and corresponding negative BO peaks are observed. The average APR_{NBO} contribution of the high-frequency *P*₃ band increases with increasing depolymerization at the expense of the BO contribution. These results are direct quantitative confirmation of the conventional assignment of the high-frequency Raman bands in depolymerized alkali silicate glasses to Si-NBO stretching vibrations. Comparison of the atomic participation ratios for *a*-SiO₂ [Fig. 6(a)] and coesite [Fig. 6(d)] shows that the general behavior of the Si and O contributions as a function of frequency in crystalline and amorphous SiO₂ structures is very similar.

5. Phase relations

The frequency dependence of the participation ratio $p_c(\omega)$ has shown that the low- and mid-frequency modes are strongly delocalized. In order to determine the character of the correlations between the individual atomic displacements, we turn to the phase quotient of the modes. The total phase quotient q_Σ is conventionally defined⁸¹ as

$$q_\Sigma(\omega_p) = \frac{\sum u_p^i \cdot u_p^j}{\sum |u_p^i \cdot u_p^j|} \quad (19)$$

which describes the extent to which the vibrational motion of the neighboring atoms is in phase (acousticlike) or out of phase (opticlike). q_Σ changes from +1 for acousticlike modes to -1 for opticlike modes.

The total phase quotient q_Σ is shown in Fig. 7 as a function of frequency. The phase quotient changes abruptly at the 500-cm⁻¹ edge and above the band gap. Previous calculations^{4,7} of q_Σ for *a*-SiO₂ also show decrease of q_Σ from +1 to -0.5 in the range 0–850 cm⁻¹, but there is no fine structure near 500 cm⁻¹ and the phase quotient of the high-frequency band has much less opticlike character. On the contrary, the phase quotient calculated by Bell and Dean⁸¹ using Born potential also exhibits minimum at about 500 cm⁻¹. It seems that the mid-frequency feature in q_Σ is a property of bond-oriented potentials.

Comparing the phase quotient of the *a*-SiO₂ and the NS4 models clearly demonstrates that the change from acousticlike modes at low frequency to opticlike modes at high frequencies is little effected by the degree of polymerization. Depolymerization leads only to a change of the modes below 100 cm⁻¹ from almost completely acoustic ($q_\Sigma \geq 0.8$) in *a*-SiO₂ to more opticlike in NS4. On the contrary, the structural disorder leads to increase of the opticlike character of the mid-frequency modes.

C. Polarized Raman spectra

The measured and calculated reduced polarized Raman spectra of the NS4 glasses are shown in Figs. 8 and 9. Details

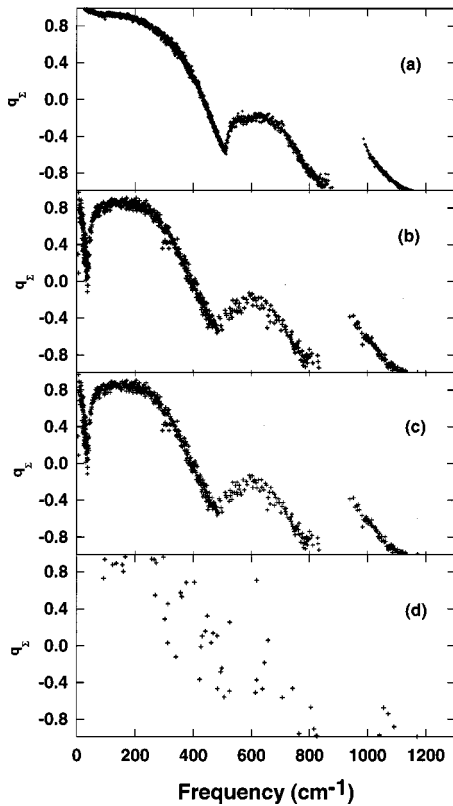


FIG. 7. Phase quotient q_z : (a) a -SiO₂; (b) NS4_I; (c) NS4_II model; (d) coesite.

of the Raman measurements are given elsewhere.³⁴ The VV spectra (Fig. 8) were normalized to have approximately the same intensity of the high-frequency peak at about 1100 cm⁻¹, while the depolarized (VH) spectra were normalized to have a similar intensity of the 800-cm⁻¹ peak.

The calculated VV spectra reproduce reasonably well the position and the relative intensities of the experimental spectrum although there are some intensity discrepancies (see below). We have used uniform Gaussian broadening with a full width at half maximum (FWHM) of 38 cm⁻¹ for all normal modes. This is the minimum broadening which results in almost featureless low-frequency bands (except for the weak feature at 380 cm⁻¹ in the NS4_I model) but it leads to an increased FWHM of the mid- and high-frequency bands as well.

Our calculations of the Raman spectra of crystalline SiO₂ polymorphs and Na₂SiO₃ have demonstrated that we were able to reproduce correctly the general order, the relative intensities, and the symmetry of the bands in the corresponding experimental spectra. Therefore the discrepancies between the calculated and the experimental Raman spectra of the NS4 glasses reflect mainly inadequacies in the corresponding structural models. The correspondence between the calculated and the experimental spectra is much better for the NS4_II model (except for the width of the 950-cm⁻¹ band) in which the Q -species distribution is closer to the experimental. In particular, the position of the 525 and 1100-cm⁻¹ bands as well as the intensity ratio I_{525}/I_{1100} are practically the same [Fig. 8(b)] *without* any additional adjustment of the bond polarizability parameters. On the contrary, the intensity of the low-frequency band in the NS4_I model is much

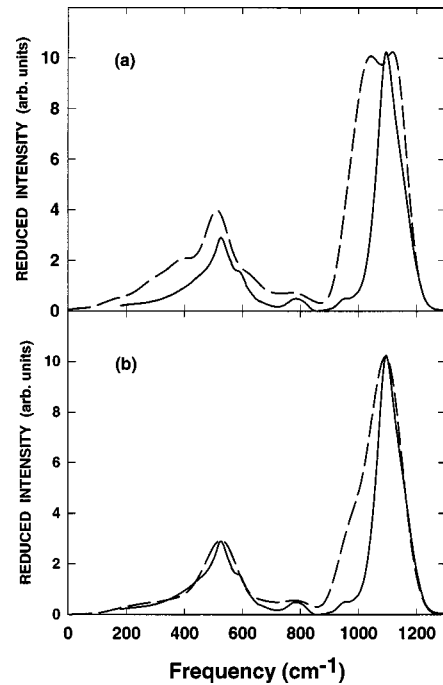


FIG. 8. VV polarized experimental (—) and calculated (---) spectra of NS4 glasses: (a) NS4_I; (b) NS4_II model.

stronger due to the presence of larger number of Q^4 species (Table V). Therefore these results clearly demonstrate that the VV spectra are very sensitive to the characteristics of the underlying structural models and the degree of polymerization.

The calculated depolarized VH spectra (Fig. 9) reproduce also most the features in the experimental VH spectrum. However, the 340- and 435-cm⁻¹ features are shifted to lower frequencies, while the 1100-cm⁻¹ band is shifted to

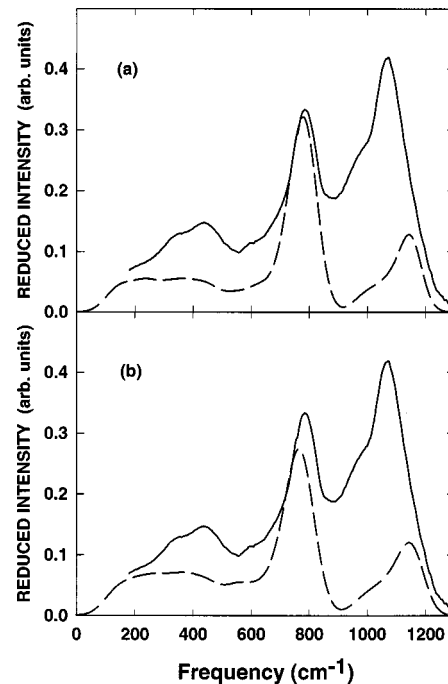


FIG. 9. VH polarized experimental (—) and calculated (---) spectra of NS4 glasses: (a) NS4_I; (b) NS4_II model.

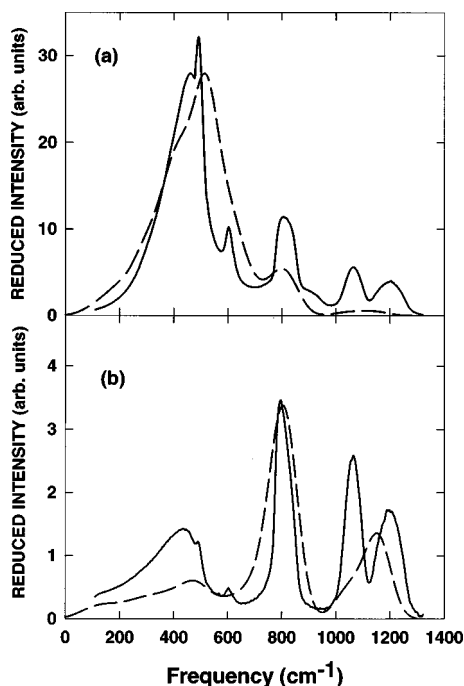


FIG. 10. Experimental (—) and calculated (···) polarized Raman spectra of a -SiO₂: (a) VV spectra; (b) VH spectra.

higher frequencies. In addition, the relative intensity of the 800-cm⁻¹ band is much stronger in the calculated spectra. The depolarized spectra are practically *insensitive* to the differences in the structural models. In this sense, their behavior is similar to that of the VDOS. The similarity between VDOS and the depolarized Raman spectra has been noticed by many authors. This can be easily understood since scattering mechanism 3, which gives the main contribution to the VH spectra, corresponds to mixed bending and stretching of the Si-O bonds both present in the VDOS.

In Fig. 10, we compare our results for a -SiO₂ with the experimentally measured in the present study reduced VV and VH spectra of a -SiO₂. The calculated VV spectrum of a -SiO₂ reproduces relatively well the overall shape of the 450-cm⁻¹ band and the intensity ratio I_{450}/I_{1100} , but the FWHM of the 450- and the 800-cm⁻¹ bands is larger and there is no splitting of the high-frequency band. Direct comparison with the previous results of Bell and Hibbins-Butler²² is not possible because they have not put the contributions from the three scattering mechanisms on a common scale. The model spectra reported in Ref. 3 using a Keating potential are very similar to our calculations for a -SiO₂ although their low-frequency VV band has extraneous sharp features at about 182, 290, 380, and 585 cm⁻¹ probably due to *insufficient* Gaussian smoothing. In both cases the calculations fail to reproduce the exact intensity and the splitting of the high-frequency bands which probably reflects some imperfections in the short-range potentials used for the calculations of the eigenvectors.

The strongest low-frequency VV Raman peak of a -SiO₂ lays between the band edges 380 and 500 cm⁻¹ in VDOS. In other words, it is predominantly due to rocking- and bending-type motions of the bridging oxygens (see Table VI).

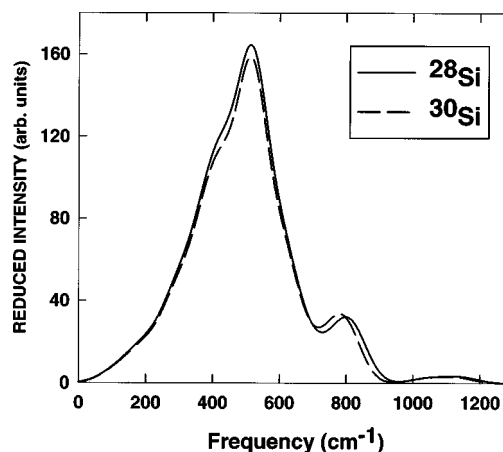


FIG. 11. Calculated VV polarized Raman spectra of a -SiO₂ for different Si isotopes: (—) ²⁸Si; (---) ³⁰Si.

The sharp D_1 and D_2 lines at 495 and 606 cm⁻¹ are not reproduced. The D_1 band is very close to the band edge separating the P_1 and the P'_1 bands in the VDOS, while the D_2 band is very close to the band edge separating P'_1 and B_2 . We have seen that the modes near the band edges are strongly localized and the position of the band edges does not strongly depend on the details of the glass structures. So it can be concluded beyond any doubt that the D_1 and D_2 bands arise from strongly localized modes. Additional studies on a -SiO₂ models with different ring distributions would be necessary in order to further address this controversial topic.

A computer simulation of the Raman spectrum of isotopically substituted a -³⁰SiO₂ (Fig. 11) reproduces exactly the isotopic shift of the 800-cm⁻¹ band reported by Galeener and Geissberger⁸² ($\Delta = -20$ cm⁻¹). This is further confirmation of the quality of our calculations, although the shift of the 450-cm⁻¹ band is slightly lower than the observed value ($\Delta_c = -4$ cm⁻¹, $\Delta_{\text{exp}} = -8$ cm⁻¹). The ³⁰Si isotopic shift of the 800-cm⁻¹ band is well explained by the large contribution of the Si atoms ($\text{APR}_{\text{Si}} \sim 0.55$) which move against the BO atoms.

The high-frequency VV Raman bands arise from the optilike stretching in character P_3 band in VDOS. In a -SiO₂ the high-frequency polarized Raman bands are very weak because the perpendicular bond polarizability $\gamma_{\text{Si-BO}}$ is small and the contribution of the neighboring BO-Si bonds to the first scattering mechanism almost cancel out each other. On the contrary, the high-frequency band in the NS4 glass is very strong although the stretching character, the bridging oxygen motion, and the phase quotient of the modes are qualitatively the same as in a -SiO₂.

D. Partial Raman spectra

In order to analyze further the character of the high-frequency polarized Raman bands in the NS4 glass, we have calculated the *partial* Raman spectra (PRS) for the different Q species (Fig. 12). The PRS of the Q^2 and Q^3 species were calculated by projecting the contribution of the Si-NBO bonds from the whole set of eigenvectors and scaling to the same number of Si atoms. The PRS of the Q^4 species were calculated by projecting the contribution of all Si-BO bonds

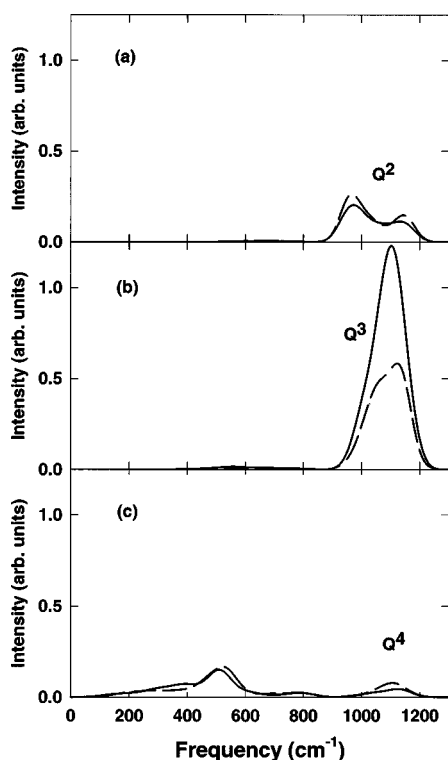


FIG. 12. Partial Raman spectra of Q^2 (a); Q^3 (b), and Q^4 (c) for: (---) NS4_I and (—) NS4_II models.

and scaling to the same number of Si atoms. Comparison of Figs. 8 and 12 shows that the strong polarized band at about 1100 cm^{-1} in the NS4 glasses arises mainly from opticlike stretching motions of the NBO atoms against the Si atoms in Q^3 units as usually assumed^{83,84} while the Si-BO contribution is much smaller. The Q^2 species exhibit a well resolved peak at about 950 cm^{-1} , as usually assumed.^{83,84} The contribution of the Q^2 and Q^3 species to the low- and mid-frequency bands is negligible except for a very weak Q^3 band at about 580 cm^{-1} . The changes in the intensity of the Q^2 and Q^3 PRS peaks are in full agreement with the Q -species distribution in the NS4 models (see Table V). The PRS intensities are proportional to the concentration of the Q^2 and Q^3 species. On the contrary, the Q^4 PRS indicate that the cross section of the Q^4 species is larger. The PRS calculations confirm and justify the use of the integral intensity of the high-frequency bands for determination of the Q species in silicate glasses and melts. The shape of the Q^2 and Q^3 PRS is, however, rather complex and direct decomposition using Gaussian components³⁴ seems to be an oversimplification.

V. SUMMARY AND CONCLUSIONS

A detailed comparison of the vibrational characteristics of sodium tetrasilicate (NS4) glass with amorphous SiO_2 ($a\text{-SiO}_2$) allows a division of the VDOS into several bands with different vibrational characteristics. The present calculations extend the band assignment of Galeener, Leadbetter, and Stringfellow⁷⁷ for $a\text{-SiO}_2$ demonstrating in particular that the $\omega_1 \rightarrow \omega_3$ band in the range $500\text{--}800\text{ cm}^{-1}$ consists, in fact, of three bands in the ranges $500\text{--}610$, $610\text{--}720$, and $720\text{--}850\text{ cm}^{-1}$, respectively.

The atomic participation ratios and the character of the BO motion are most sensitive to the degree of polymerization because they depend on the concentration of the atomic species present. Qualitatively, the general character of the different vibrational modes remains the same with increasing degree of depolymerization. This implies that the vibrational properties of silicate glasses are local phenomena reflecting the rigidity of the corner-sharing SiO_4 tetrahedra. Nevertheless, depolymerization does lead to several important effects—the appearance of new Na and NBO bands, increase of the localization of the low- and mid-frequency modes, as well as quantitative changes in the contribution of the different atoms to the normal modes.

The strong VV polarized bands at about 525 and 1100 cm^{-1} in the spectrum of the NS4 glass originate almost entirely from polarizability changes due to bond stretching (compression). On the contrary, the depolarized Raman spectra arise from mixed bending+stretching scattering mechanism. The bond polarizabilities parameters of the silicon—BO bonds are not strongly affected by structural disorder when going from crystalline to amorphous silicates. The strong intensity increase of the high-frequency polarized Raman bands in depolymerized glasses reflects the increase in the derivative of the parallel bond polarizability of the silicon-NBO bonds.

The calculated partial VV polarized Raman spectra for different Q species confirm the usual empirical assignments of the 950-cm^{-1} band to Q^2 species and the 1100-cm^{-1} band to Q^3 units and quantitatively shows that their cross sections are the same. But their actual shape is rather complex and they strongly overlap. This suggests that the usual Gaussian decomposition of the high-frequency bands of alkali silicate glasses into different Q species contributions is an oversimplification, probably correct only for narrow compositional ranges.

The places where the calculations of the Raman spectra failed are due to different reasons. The first reason is related to the limitations in the potential model and in the calculation procedures used. Additional systematic studies of the effects of different interatomic potentials on the Raman spectra calculations are necessary. Similarly, improvements of the Raman intensity calculations, in particular introduction of dependence of the parallel bond polarizability on the bond length and nonuniform broadening, are desirable.

The second kind of discrepancies is associated with the quality of the structural models themselves. Calculations on glass models with still better Q -species distributions would be necessary to constrain better the actual shape of the Q^2 and Q^3 peaks. Calculations on SiO_2 and NS4 models with a different number of three- and four-membered rings would be necessary to further test the assignment of the D_1 and D_2 bands, postulated by Galeener.⁷⁵

In any case, the results presented demonstrate that calculations of the dynamics of silicate glass models should not stop with the calculation of the VDOS and VH Raman spectra, because they are not very sensitive to the details of the glass structure, but should proceed to compute the VV polarized Raman spectra, which represent a stringent test for constructing more realistic glass models.

- ¹R. J. Bell, N. F. Bird, and P. Dean, *J. Phys. C* **1**, 299 (1968).
- ²L. Guttman and S. Rahman, *J. Non-Cryst. Solids* **75**, 419 (1985).
- ³R. A. Murray and W. Y. Ching, *Phys. Rev. B* **39**, 1320 (1989).
- ⁴W. Jin, P. Vashishta, R. K. Kalia, and J. P. Rino, *Phys. Rev. B* **48**, 9359 (1993).
- ⁵J. Sarnthein, A. Pasquarello, and R. Car, *Science* **275**, 1975 (1997).
- ⁶K. Vollmayr, W. Kob, and K. Binder, *Phys. Rev. B* **54**, 15 808 (1996).
- ⁷S. N. Taraskin and S. R. Elliott, *Phys. Rev. B* **56**, 8605 (1997).
- ⁸M.-Z. Huang, L. Ouyang, and W. Y. Ching, *Phys. Rev. B* **59**, 3540 (1999).
- ⁹S. H. Garofalini, *J. Chem. Phys.* **76**, 3189 (1982); *J. Non-Cryst. Solids* **120**, 1 (1990).
- ¹⁰S. K. Mitra, *Philos. Mag. B* **45**, 529 (1982).
- ¹¹A. Alavi, L. J. Alvarez, S. R. Elliott, and I. R. McDonald, *Philos. Mag. B* **65**, 489 (1992).
- ¹²I. P. Swainson and M. T. Dove, *Phys. Rev. Lett.* **71**, 193 (1993).
- ¹³R. G. Della Valle and E. Venuti, *Chem. Phys.* **179**, 411 (1994).
- ¹⁴R. B. Laughlin and J. D. Joannopoulos, *Phys. Rev. B* **16**, 2942 (1977).
- ¹⁵R. A. Barrio, F. L. Galeener, and E. Martinez, *Phys. Rev. B* **31**, 7779 (1985).
- ¹⁶P. N. Sen and M. F. Thorpe, *Phys. Rev. B* **15**, 4030 (1977).
- ¹⁷F. L. Galeener, *Phys. Rev. B* **19**, 4292 (1979); M. F. Thorpe and F. L. Galeener, *ibid.* **22**, 3078 (1980).
- ¹⁸R. Shuker and R. W. Gammon, *Phys. Rev. Lett.* **25**, 222 (1970); *Phys. Lett.* **33A**, 96 (1970); *J. Chem. Phys.* **55**, 4784 (1971).
- ¹⁹F. L. Galeener and P. N. Sen, *Phys. Rev. B* **17**, 1928 (1978).
- ²⁰R. M. Martin and F. L. Galeener, *Phys. Rev. B* **23**, 3071 (1981).
- ²¹R. J. Bell and D. C. Hibbins-Butler, *J. Phys. C* **9**, 1171 (1976).
- ²²R. J. Bell and D. C. Hibbins-Butler, *J. Phys. C* **9**, 2955 (1976).
- ²³M. Wilson, P. A. Madden, M. Hemmati, and C. A. Angell, *Phys. Rev. Lett.* **77**, 4023 (1996).
- ²⁴A. Pasquarello and R. Car, *Phys. Rev. Lett.* **79**, 1766 (1997).
- ²⁵P. H. Gaskell, *Phys. Chem. Glasses* **8**, 69 (1967); *Trans. Faraday Soc.* **62**, 1493 (1966).
- ²⁶E. Dowty, *Phys. Chem. Miner.* **14**, 67 (1987), and references therein.
- ²⁷S. A. Brawer, *Phys. Rev. B* **11**, 3173 (1975); S. A. Brawer and W. B. White, *J. Chem. Phys.* **63**, 2421 (1975).
- ²⁸T. Furukawa, K. E. Fox, and W. B. White, *J. Chem. Phys.* **75**, 3226 (1981).
- ²⁹M. Marinov, N. Zotov, B. Mihailova, J. Nikolov, and L. Konstantinov, *J. Phys.: Condens. Matter* **6**, 3813 (1994).
- ³⁰N. Zotov, M. Marinov, and L. Konstantinov, *J. Non-Cryst. Solids* **197**, 179 (1996).
- ³¹T. Uchino, Y. Tokuda, and T. Yoko, *Phys. Rev. B* **58**, 5322 (1998).
- ³²N. Zotov, H. Keppler, A. C. Hannon, and A. K. Soper, *J. Non-Cryst. Solids* **202**, 153 (1996).
- ³³N. Zotov, R. Delaplane, and H. Keppler, *Phys. Chem. Miner.* **26**, 107 (1998).
- ³⁴N. Zotov and H. Keppler, *Phys. Chem. Miner.* **25**, 259 (1998).
- ³⁵D. W. Matson, S. K. Sharma, and J. A. Philpotts, *J. Non-Cryst. Solids* **58**, 323 (1983).
- ³⁶F. Gervais, A. Blin, and M. H. Chipinet, *Solid State Commun.* **65**, 653 (1988).
- ³⁷X. Xu, J. F. Stebbins, M. Kanzaki, P. F. McMillan, and B. Poe, *Am. Mineral.* **76**, 8 (1991).
- ³⁸G. H. Wolf, D. J. Durben, and P. F. McMillan, *J. Chem. Phys.* **93**, 2280 (1990).
- ³⁹B. O. Mysen and J. D. Frantz, *Eur. J. Mineral.* **5**, 393 (1993); *Contrib. Mineral. Petrol.* **117**, 1 (1994).
- ⁴⁰R. Duprtee, D. Holland, P. W. McMillan, and R. F. Pettifer, *J. Non-Cryst. Solids* **68**, 399 (1984).
- ⁴¹J. F. Emerson, P. E. Stallworth, and P. J. Bray, *J. Non-Cryst. Solids* **113**, 253 (1989).
- ⁴²H. Maekawa, T. Maekawa, K. Kawamura, and T. Yokokawa, *J. Non-Cryst. Solids* **127**, 53 (1991).
- ⁴³J. Kümmerlen, L. H. Merwin, A. Sebald, and H. Keppler, *J. Phys. Chem.* **96**, 6405 (1992).
- ⁴⁴B. W. H. van Beest, G. J. Kramer, and R. A. van Santen, *Phys. Rev. Lett.* **64**, 1955 (1990).
- ⁴⁵S. Tsuneyuki, M. Tsukada, H. Aoki, and Y. Matsui, *Phys. Rev. Lett.* **61**, 869 (1988).
- ⁴⁶B. Vessal, A. Amini, D. Fincham, and C. R. A. Catlow, *Philos. Mag. B* **60**, 753 (1989); B. Vessal, G. N. Greaves, P. T. Marten, A. V. Chadwick, R. Mole, and S. Houde-Walter, *Nature (London)* **356**, 504 (1992).
- ⁴⁷P. Vashishta, P. K. Kalia, J. P. Rino, and I. Ebbsjö, *Phys. Rev. B* **41**, 12 197 (1990).
- ⁴⁸B. Michailova, N. Zotov, M. Marinov, J. Nikolov, and L. Konstantinov, *J. Non-Cryst. Solids* **168**, 265 (1994).
- ⁴⁹D. A. Long, *Raman Spectroscopy* (McGraw-Hill, New York, 1977).
- ⁵⁰R. Alben, D. Weaire, J. E. Smith, Jr., and M. H. Brodsky, *Phys. Rev. B* **11**, 2271 (1975).
- ⁵¹E. R. Lippincott and J. M. Stutman, *J. Phys. Chem.* **68**, 2926 (1964).
- ⁵²W. G. Fateley, F. R. Dollish, N. T. McDevitt, and F. F. Bentley, *Infrared and Raman Selection Rules for Molecules and Lattice Vibrations: The Correlation Method* (Wiley-Interscience, New York, 1972).
- ⁵³J. F. Scott and S. P. S. Porto, *Phys. Rev.* **161**, 903 (1967).
- ⁵⁴J. N. Plendl, L. C. Mansur, A. Hadni, F. Brehat, P. Henry, G. Morlot, F. Naudin, and P. Strimer, *J. Phys. Chem. Solids* **28**, 1589 (1967).
- ⁵⁵J. B. Bates and A. S. Quist, *J. Chem. Phys.* **56**, 1528 (1972).
- ⁵⁶J. B. Bates, *J. Chem. Phys.* **57**, 4042 (1972).
- ⁵⁷M. Ocana, V. Fornes, J. V. Garcia-Ramos, and C. R. Serna, *Phys. Chem. Miner.* **14**, 527 (1987).
- ⁵⁸S. K. Sharma, J. F. Mammone, and M. F. Nicol, *Nature (London)* **292**, 140 (1981).
- ⁵⁹P. Gillet, A. Le Cleach, and M. Madon, *J. Geophys. Res.* **95**, 21 635 (1990).
- ⁶⁰J. Wong and C. A. Angell, *Glass Structure by Spectroscopy* (Marcel Dekker, New York, 1976).
- ⁶¹P. Richet, B. O. Mysen, and D. Andrault, *Phys. Chem. Miner.* **23**, 157 (1996).
- ⁶²J. B. Bates, *J. Chem. Phys.* **56**, 1910 (1972).
- ⁶³D. Beeman and R. Alben, *Adv. Phys.* **26**, 339 (1977).
- ⁶⁴C. W. Gear, *Numerical Initial Value Problems in Ordinary Differential Equations* (Prentice Hall, New York, 1971).
- ⁶⁵B. P. Feuston and S. H. Garofalini, *J. Chem. Phys.* **89**, 5818 (1988).
- ⁶⁶D. Timpel, K. Scheerschmidt, and S. H. Garofalini, *J. Non-Cryst. Solids* **221**, 187 (1997).
- ⁶⁷D. Timpel and K. Scheerschmidt, *J. Non-Cryst. Solids* **232–234**, 245 (1998).

- ⁶⁸G. T. Barkema and N. Mousseau, *Phys. Rev. Lett.* **77**, 4358 (1996).
- ⁶⁹W. S. McDonalds and D. W. J. Cruickshank, *Acta Crystallogr.* **22**, 37 (1967).
- ⁷⁰A. K. Pant and D. W. J. Cruickshank, *Acta Crystallogr., Sect. B: Struct. Crystallogr. Cryst. Chem.* **24**, 13 (1968).
- ⁷¹R. L. Mozzi and B. E. Warren, *J. Appl. Crystallogr.* **2**, 164 (1969).
- ⁷²P. H. Gaskell and I. D. Tarrant, *Philos. Mag. B* **42**, 265 (1980).
- ⁷³H. Konnert and J. Karle, *Acta Crystallogr., Sect. A: Cryst. Phys., Diffraction, Theor. Gen. Crystallogr.* **29**, 702 (1973).
- ⁷⁴A. C. Wright and R. N. Sinclair, *J. Non-Cryst. Solids* **76**, 351 (1985).
- ⁷⁵F. L. Galeener, *J. Non-Cryst. Solids* **49**, 53 (1982).
- ⁷⁶A. Pasquarello and R. Car, *Phys. Rev. Lett.* **80**, 5145 (1998).
- ⁷⁷F. L. Galeener, A. J. Leadbetter, and M. W. Stringfellow, *Phys. Rev. B* **27**, 1052 (1983).
- ⁷⁸J. M. Carpenter and D. L. Price, *Phys. Rev. Lett.* **54**, 441 (1985); D. L. Price and J. M. Carpenter, *J. Non-Cryst. Solids* **92**, 153 (1987).
- ⁷⁹R. J. Bell, P. Dean, and D. C. Hibbins-Butler, *J. Phys. C* **3**, 2111 (1970).
- ⁸⁰R. J. Bell, P. Dean, and D. C. Hibbins-Butler, *J. Phys. C* **4**, 1214 (1971).
- ⁸¹R. J. Bell and D. C. Hibbins-Butler, *J. Phys. C* **8**, 787 (1975).
- ⁸²F. L. Galeener and A. E. Geissberger, *Phys. Rev. B* **27**, 6199 (1983).
- ⁸³P. McMillan, *Am. Mineral.* **69**, 622 (1984).
- ⁸⁴P. F. McMillan and G. H. Wolf, *Rev. Mineral.* **32**, 247 (1995).
- ⁸⁵A. Pasquarello, J. Sarnthein, and R. Car, *Phys. Rev. B* **57**, 14 133 (1998).